



# CH<sub>4</sub>-CO<sub>2</sub> replacement in hydrate-bearing sediments: A pore-scale study

J. W. Jung and J. Carlos Santamarina

*School of Civil and Environmental Engineering, Georgia Institute of Technology, 790 Atlantic Drive, NW, Atlanta, Georgia 30332-0355, USA (jjung7@mail.gatech.edu)*

[1] The injection of CO<sub>2</sub> into CH<sub>4</sub> hydrate-bearing sediments causes the release of CH<sub>4</sub> and the formation of CO<sub>2</sub> hydrate within the CH<sub>4</sub> hydrate stability field. CH<sub>4</sub>-CO<sub>2</sub> replacement allows for the recovery of an energy source, CH<sub>4</sub>, while trapping CO<sub>2</sub>. In this study, we monitor pore-scale changes in electrical resistance and relative stiffness during CH<sub>4</sub> hydrate formation, CH<sub>4</sub>-CO<sub>2</sub> replacement, and hydrate dissociation; experiments are also observed using high-resolution time-lapsed photography. Results show that CH<sub>4</sub>-CO<sub>2</sub> replacement occurs locally and gradually so that the overall hydrate mass remains solid and no stiffness loss should be expected at the sediment scale. Other experimental results confirm the slow diffusion of CH<sub>4</sub> through the hydrate shell that forms between water and gas; this may allow for the coexistence of gas-hydrate-water phases for long periods of time.

**Components:** 3100 words, 4 figures.

**Keywords:** CH<sub>4</sub> hydrate; CH<sub>4</sub>-CO<sub>2</sub> replacement; energy; CO<sub>2</sub> hydrate.

**Index Terms:** 3004 Marine Geology and Geophysics: Gas and hydrate systems; 3022 Marine Geology and Geophysics: Marine sediments: processes and transport.

**Received** 23 August 2010; **Revised** 4 October 2010; **Accepted** 11 October 2010; **Published** 11 December 2010.

Jung, J. W., and J. C. Santamarina (2010), CH<sub>4</sub>-CO<sub>2</sub> replacement in hydrate-bearing sediments: A pore-scale study, *Geochem. Geophys. Geosyst.*, 11, Q0AA13, doi:10.1029/2010GC003339.

**Theme:** EarthTime: Advances in Geochronological Technique

**Guest Editors:** D. Condon, G. Gehrels, M. Heizler, and F. Hilgen

## 1. Introduction

[2] Worldwide carbon reserves in the form of CH<sub>4</sub> hydrate are on the order of 500–10,000 Gt [Collett, 2002; Kvenvolden, 1988; Milkov, 2004; Ruppel and Pohlman, 2008]. The injection of CO<sub>2</sub> into CH<sub>4</sub> hydrate-bearing sediments has the advantage of liberating CH<sub>4</sub> while simultaneously sequestering CO<sub>2</sub> leading to the more sustainable use of a fossil fuel [McGrail *et al.*, 2007; Ota *et al.*, 2005; Stevens *et al.*, 2008; Svandal *et al.*, 2006; Zhou *et al.*, 2008].

[3] The extent of the CH<sub>4</sub>-CO<sub>2</sub> replacement is affected by multiple factors and coexisting processes, such as pressure- and temperature-dependent relative viscosity, permeability, density and solubilities among water, CH<sub>4</sub> and CO<sub>2</sub> [Jung *et al.*, 2010]. Previous studies have observed no apparent dissociation during replacement [Stevens *et al.*, 2008], and have monitored replacement ratios and rates which show that the CH<sub>4</sub>-CO<sub>2</sub> replacement rate increases near the CH<sub>4</sub> hydrate phase boundary and with increasing CO<sub>2</sub> gas pressure, reaching a constant value when the CO<sub>2</sub> liquefies [McGrail *et al.*,

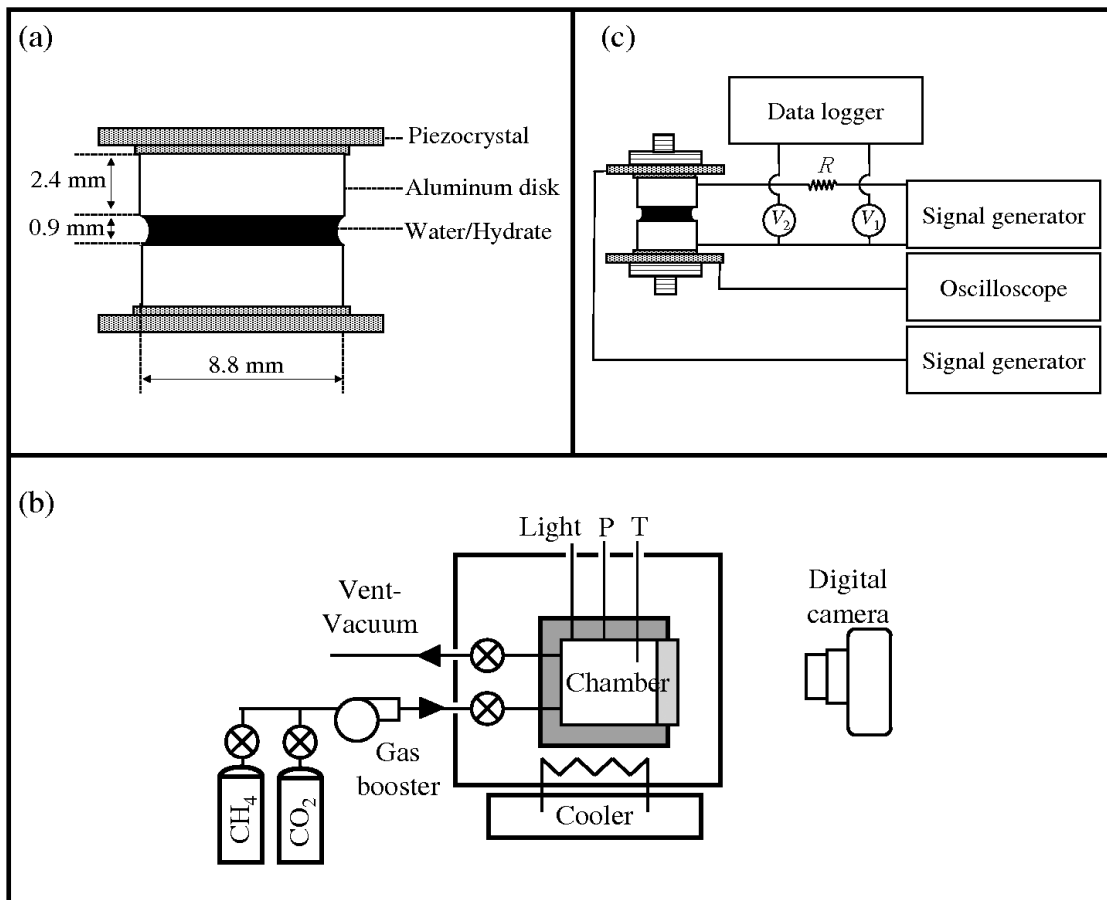


**Figure 1.** Experimental devices and components: (a) pore-scale device, (b) pressure chamber and external components, and (c) peripheral electronics to measure electrical conductivity and relative stiffness.

2007; Ota *et al.*, 2005, 2007]. The replacement ratio increases when a mixture of CO<sub>2</sub> and N<sub>2</sub> is used for replacement because the smaller N<sub>2</sub> molecule facilitates the replacement of CH<sub>4</sub> from the small cage in structure I hydrate [Park *et al.*, 2006].

[4] The stability of hydrate-bearing sediments during CH<sub>4</sub>-CO<sub>2</sub> replacement is not yet well understood. In this study, we monitor pore-scale changes in electrical resistance and stiffness to gain an in-depth view of ongoing process. We choose these measurements because of the pronounced sensitivity of underlying physical parameters to phase changes. In particular, the electrical resistivities of water, hydrate, liquid CO<sub>2</sub> and CH<sub>4</sub> gas are ordered as  $\rho_{H_2O} < \rho_{hyd} < \rho_{CO_2-liquid} < \rho_{CH_4gas}$  from  $\rho \sim 0.2 \Omega \text{ m}$  for seawater to  $\rho \sim \infty$  for gas. On the other hand, stiffness ranks as follows  $B_{CH_4gas} < B_{CO_2-liquid} < B_{H_2O} < B_{hyd}$  (note that the bulk modulus of liquid CO<sub>2</sub> is almost one order of magnitude lower than that of water). These

observations guide the design of the device and test methodology used in this study.

## 2. Experimental Study

[5] The experimental device is designed to explore hydrate formation and CH<sub>4</sub>-CO<sub>2</sub> replacement at a small scale, such as at the water meniscus that forms between particles in a partially water-saturated sediment.

### 2.1. Device

[6] The test consists of a thin cylindrical water layer (8.8 mm diameter, 0.9 mm in height; and 55 mg water mass) retained by surface tension between two conductive aluminum disks (Figure 1a). These disks are bonded onto corresponding piezocrystals. The device is housed in a high-pressure chamber within a temperature controlled environ-

ment (Figure 1b). The water droplet is recorded using time-lapse photography to confirm phase changes and to observe volume changes (resolution: 1 pixel $\sim$ 10  $\mu$ m). Pressure and temperature are measured with a pressure transducer and a thermocouple, respectively, and values are recorded every 2 s using a data logger.

[7] Figure 1c shows the electrical circuit and peripheral electronics used to measure electrical resistance and relative stiffness. Electrical resistance is determined at 50 kHz to avoid electrode polarization effects. The resistance of the medium  $R$  is a function of measured voltages  $V_1$  and  $V_2$ , and the known resistance of the series resistor  $R^* = 4700 \Omega$ ,

$$R = \frac{V_2}{V_1 - V_2} R^* \quad (1)$$

The source piezocrystal is connected to a sinusoidal signal generator operated at  $\sim$ 60 kHz. The signal amplitude produced by the output piezocrystal is measured using an oscilloscope.

## 2.2. Experimental Procedure

[8] Multistage P-T trajectories are imposed in three different experiments. For clarity, a single, complete test sequence is reported in this manuscript. Similar results were obtained in all other tests. The P-T trajectory during this experiment consists of three stages (Figure 2): (1) ice formation and melting followed by CH<sub>4</sub> hydrate formation, (2) CH<sub>4</sub>-CO<sub>2</sub> replacement, and (3) hydrate dissociation. Details for each stage follow.

### 2.2.1. Transient Ice Formation

[9] A droplet of deaired water ( $\rho_w = 231 \Omega$  m) is placed between the two aluminum substrates, creating a cylindrically shaped meniscus (see Figure 2a). The chamber is briefly vacuumed, then pressurized with CH<sub>4</sub> gas to 8.1 MPa and kept at a temperature  $\sim$ 277°K for 11 h under quiescent conditions. The pressure and temperature are rapidly decreased to 3.7 MPa and 250°K to form ice (some hydrate may form as well).

### 2.2.2. CH<sub>4</sub> Hydrate Formation

[10] Within 2 min after partial depressurization, pressure and temperature are increased back to 7.6 MPa and 277°K, to melt the ice within the CH<sub>4</sub> hydrate stability field (see Figure 2a). These P-T values are maintained constant for 23 h to allow for CH<sub>4</sub> hydrate growth.

### 2.2.3. Injection of CO<sub>2</sub>

[11] CH<sub>4</sub> gas is allowed to leak out of the chamber, and P-T condition is maintained inside of the CH<sub>4</sub> hydrate stability field, while CO<sub>2</sub> is injected into the chamber (see Figure 2b). Eventually the hydrate mass is submerged in liquid CO<sub>2</sub>. Pressure and temperature are kept at  $P = 7$  MPa and  $T = 276$  °K for 19 h.

### 2.2.4. Hydrate Dissociation

[12] Depressurization is conducted in three steps: from liquid CO<sub>2</sub> to gas CO<sub>2</sub> (points c0 to c1 in Figure 2c), between CH<sub>4</sub> and CO<sub>2</sub> phase boundaries (points c2 to c3 in Figure 2c), and out of the CO<sub>2</sub> hydrate stability field (points c3 to c4 in Figure 2c).

## 3. Experimental Results

[13] Similar results were obtained in all three multistage tests. For clarity, a data set from a single complete test is reported here. Pressure, temperature, electrical resistance  $R$  and relative stiffness  $K$  measured during the tests are summarized in Figure 3. All parameters are plotted versus time. Note that time is zeroed at the center of the main process under consideration in each column, and plotted using a cubic root scale to show short-time effects in high resolution together with long-time changes. The evolution of the water droplet photographed through the sapphire window is documented in Figure 4 (for clarity, we show traces of the original photographs).

### 3.1. Transient Ice Formation

[14] A pronounced increase in resistance and stiffness accompany ice formation (Figure 3a). There is only a minor volume change (Figure 4b).

### 3.2. CH<sub>4</sub> Hydrate Formation

[15] Ice melts and CH<sub>4</sub> hydrate starts forming upon repressurization back inside CH<sub>4</sub> hydrate stability field. The electrical resistance  $R$  and relative stiffness  $K$  decrease fast as the ice melts (between points a2 and a3 in Figure 3a). Therefore, there is virtually no hydrate formation during ice melting even though P-T conditions are within the hydrate stability field. This suggests that thermal diffusion-limited ice melting is much faster than gas diffusion-controlled hydrate formation.

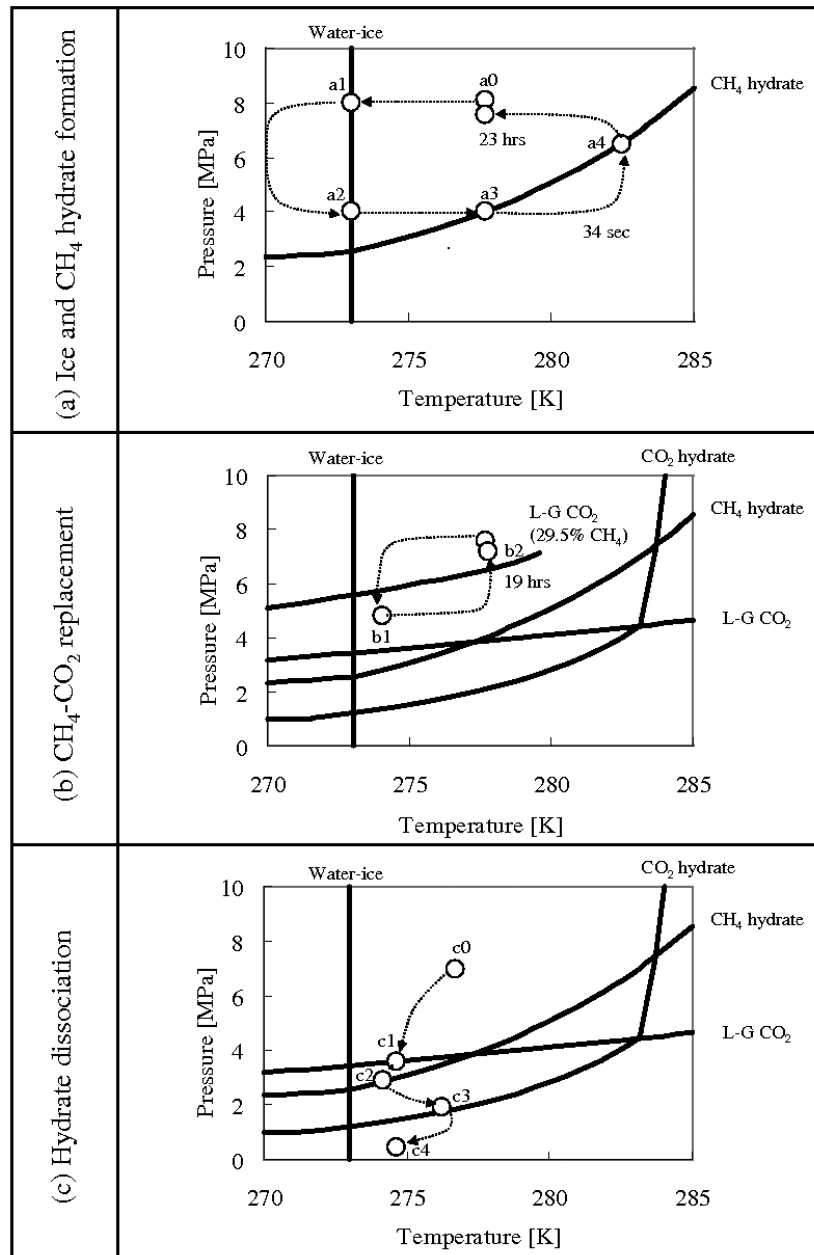


**Figure 2.** Complete P-T history during the experiment: water (point a0), ice forms (point a1), ice melts (point a2), leaving the CH<sub>4</sub> hydrate phase boundary (point a3), CH<sub>4</sub> hydrate nucleation and growth (point a4), CO<sub>2</sub> injection (point b1), liquid CO<sub>2</sub> forms in the chamber (point b2), beginning of depressurization (point c0), gas-liquid CO<sub>2</sub> phase boundary (point c1), CH<sub>4</sub> hydrate phase boundary (point c2), CO<sub>2</sub> hydrate phase boundary (point c3), and end of test (point c4).

[16] Any hydrate that may have formed dissociates between points a3 and a4 (Figures 2 and 3a), then both resistance  $R$  and stiffness  $K$  begin to gradually increase during CH<sub>4</sub> hydrate formation (after point a4 in Figure 3, duration 23 h), however, neither resistance nor stiffness reach the values attained during ice formation. Volume expansion during

hydrate growth causes water to flow out of the meniscus, and some hydrate forms on the aluminum surface (Figure 4c).

### 3.3. Injection of CO<sub>2</sub>

[17] Minor changes in electrical resistance  $R$  and relative stiffness  $K$  are observed during the injec-

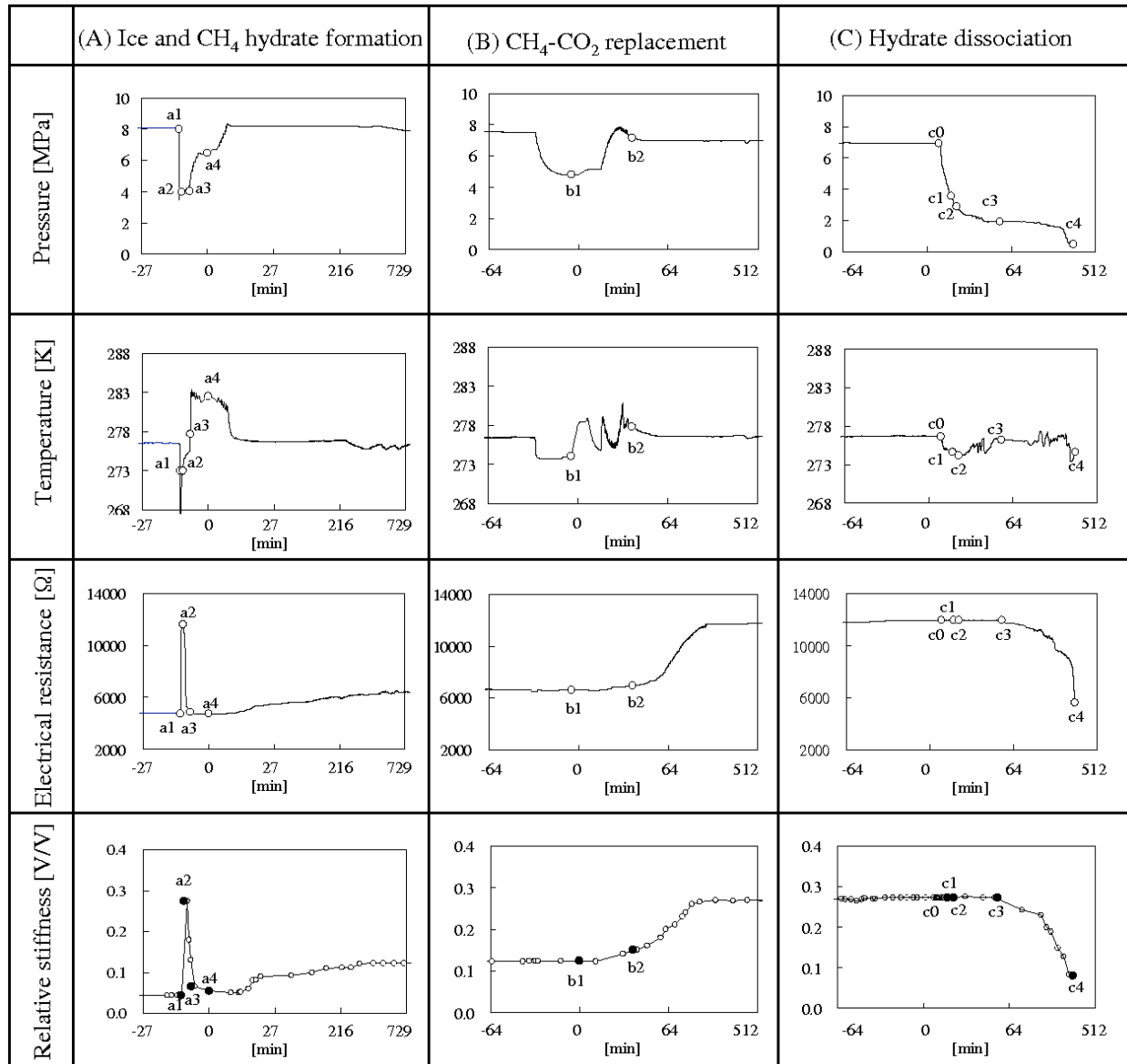


**Figure 3.** Evolutions of pressure, temperature, electrical resistance, and relative stiffness during all experiments at stages (refer to Figure 2 for detailed P-T path): water (point a0), ice forms (point a1), ice melts (point a2), leaving the CH<sub>4</sub> hydrate phase boundary (point a3), CH<sub>4</sub> hydrate nucleation and growth (point a4), CO<sub>2</sub> injection (point b1), liquid CO<sub>2</sub> forms in the chamber (point b2), beginning of depressurization (point c0), gas-liquid CO<sub>2</sub> phase boundary (point c1), CH<sub>4</sub> hydrate phase boundary (point c2), CO<sub>2</sub> hydrate phase boundary (point c3), and end of test (point c4). Note that a cubic time scale is used to capture long time scale together with high time resolution near critical events.

tion of CO<sub>2</sub> gas (Figure 3, points b1 to b2 (note that this is confirmed in all our tests)). However, resistance  $R$  and stiffness  $K$  increase fast as soon as liquid CO<sub>2</sub> conditions are exceeded [see also *Ota et al.*, 2007]. Both  $K$  and  $R$  reach values higher than during CH<sub>4</sub> hydrate formation (point b2 in Figure 3). The mixed CH<sub>4</sub>-CO<sub>2</sub> gas leads to a modified G-L CO<sub>2</sub> boundary, and liquid CO<sub>2</sub>

forms above the liquid-gas P-T condition for pure CO<sub>2</sub> (Figure 2, point b2 (see related data given by *Donnelly and Katz* [1954])).

### 3.4. Hydrate Dissociation

[18] Depressurization from liquid CO<sub>2</sub> to gas CO<sub>2</sub>, and out of the CH<sub>4</sub> phase boundary, causes no

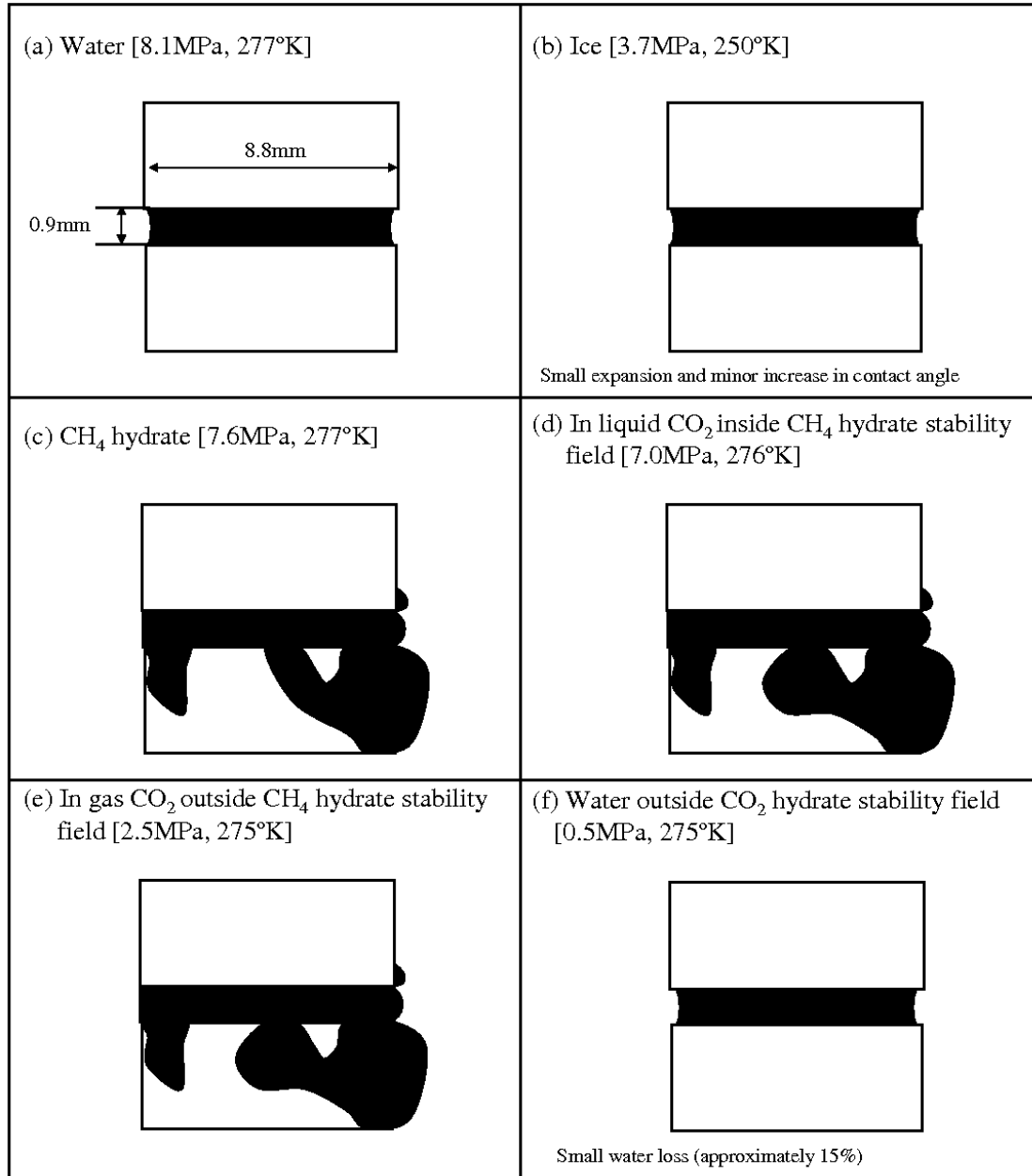


**Figure 4.** Traces of photographs obtained during the replacement: (a) water droplet, (b) ice formation, (c) CH<sub>4</sub> hydrate formation and growth, (d) after the injection of liquid CO<sub>2</sub>, (e) depressurization out of the CH<sub>4</sub> hydrate stability field, and (f) image after hydrate dissociation.

observable change in the electrical resistance  $R$  and relative stiffness  $K$ . Therefore, we infer that CO<sub>2</sub> hydrate fills the meniscus (Figure 3, points c1 and c2). Finally, hydrate dissociates at the CO<sub>2</sub> hydrate phase boundary (Figures 2 and 3, point c3). As hydrate dissociates, resistance  $R$  and stiffness  $K$  return to the initial values measured for the water droplet at the beginning of the test. The water loss from the

beginning to the end of the test is estimated to be ~15% based on the photographic record.

## 4. Analyses and Discussion

### 4.1. Volume Expansion

[19] There is pronounced volume expansion during CH<sub>4</sub> hydrate formation; a theoretical estimate

shows that  $V_{\text{CH}_4\text{hyd}}/V_w = 1.23$  for a hydration number  $n = 6$ . Volume expansion causes water to flow out of the meniscus, readily forming hydrate on the sides of the aluminum block (Figure 4c).  $\text{CH}_4\text{-CO}_2$  replacement and additional  $\text{CO}_2$  hydrate formation of any remaining free water inside the meniscus can cause additional volume expansion as seen in Figure 4d ( $V_{\text{CO}_2\text{hyd}}/V_w = 1.28$ ). Note that the volume of  $\text{CO}_2$  hydrate is slightly larger than for  $\text{CH}_4$  hydrate ( $V_{\text{CO}_2\text{hyd}}/V_{\text{CH}_4\text{hyd}} = 1\% \text{--} 6\%$  [Jung *et al.*, 2010]).

## 4.2. Relative Stiffness

[20] Relative stiffness measurements can be analyzed assuming a mechanical system made of three springs in series held between fixed boundaries: the two end springs represent the two piezocrystals, and the central spring corresponds to the meniscus (either water, ice or hydrate). Infinite stiffness connectors between the springs represent the two aluminum disks. The relative amplitude between the input  $V_i$  and output  $V_o$  voltages is a function of the displacement  $\delta_i$  and  $\delta_o$  in both input and output piezocrystals, which depends on the meniscus response  $\delta_m = -\delta_o - \delta_i$  through a function that combines the stiffness of piezocrystals  $k_{\text{piezo}}$ , the meniscus height ( $L_m = 0.9$  mm), the medium Young's modulus  $E_m$ , and the area of the meniscus  $A_m = 60.8$  mm<sup>2</sup>,

$$\frac{V_o}{V_i} = \alpha \frac{\delta_o}{\delta_i} = \alpha \frac{\delta_o}{\delta_o + \delta_m} = \alpha \frac{1}{1 + \frac{k_{\text{piezo}}L}{E_m A_m}} \quad (2)$$

where  $\alpha$  is the ratio between the mechanoelectric and electromechanical piezocrystal effects. Parameters  $\alpha$  and  $k_{\text{piezo}}$  are inferred by assuming known condition at 100% ice and 100%  $\text{CO}_2$  hydrate ( $\alpha = 1.39$  and  $k_{\text{piezo}} = 2.62 \times 10^9$  N/m assuming  $E_{\text{ice}} = 9.5$  GPa and  $E_{\text{hyd}} = 8.4$  GPa). Equation (2) shows that the voltage ratio  $V_o/V_i$  is indeed a measure of meniscus stiffness  $E_m A_m/L_m$  relative to the stiffness of piezocrystals  $k_{\text{piezo}}$ . The  $\text{CH}_4$  hydrate mass obtained using the measured voltage ratio  $(V_o/V_i)_{\text{CH}_4\text{hyd}} = 0.129$  is 47% of the meniscus volume.

## 4.3. Electrical Resistance

[21] Electrical resistance  $R$  is a function of resistivity  $\rho$ , meniscus length  $L_m$ , area  $A_m$ , and a shape factor  $\beta$ ,

$$R = \beta \cdot \rho \frac{L_m}{A_m} \quad (3)$$

When an annular  $\text{CH}_4$  hydrate shell forms, the measured resistance reflects the contributions of water and hydrate in parallel disregarding ion exclusion.

$$\begin{aligned} \frac{1}{R_{\text{water+hyd}}} &= \frac{1}{R_{\text{hyd}}} + \frac{1}{R_{\text{water}}} \\ &= \frac{1}{\beta \cdot L} \left( \frac{A_{\text{total}} - A_{\text{water}}}{\rho_{\text{hyd}}} + \frac{A_{\text{water}}}{\rho_{\text{water}}} \right) \quad (4) \\ &\approx \frac{1}{L} \frac{A_{\text{water}}}{\rho_{\text{water}}} \end{aligned}$$

where the final approximation applies to a shape factor  $\beta = 1$  for a short cylinder and a ratio of resistivities  $\rho_{\text{ice}}/\rho_{\text{water}} \approx \rho_{\text{hyd}}/\rho_{\text{water}} \ll 1.0$ . For an initial water resistivity  $\rho_{\text{water}} = 231$   $\Omega$  m measured before  $\text{CH}_4$  hydrate formation, a lower bound estimated (disregarding ion exclusion) of the  $\text{CH}_4$  hydrate volume is 48% of the total meniscus volume. We conclude that (1) a significant part of the meniscus remains as free water 23 h after the initiation of  $\text{CH}_4$  hydrate formation and (2) the computed  $\text{CH}_4$  hydrate growth rate confirms that  $\text{CH}_4$  hydrate formation is  $\text{CH}_4$  diffusion-limited through the annular hydrate shell ( $\text{CH}_4$  gas diffusivity through  $\text{CH}_4$  hydrate  $7.6 \times 10^{-13}$  m<sup>2</sup>/s [Davies *et al.*, 2008]).

## 4.4. Replacement

[22] Both relative stiffness and electrical resistance increase at all times during replacement. Therefore, while the transformation requires the opening of the hydrate cage to release the  $\text{CH}_4$  and entrap the  $\text{CO}_2$  molecule [Jung *et al.*, 2010], this solid-liquid-solid exchange takes place locally at the reaction front, while the rest of the hydrate mass remains solid. Therefore, no stiffness loss should be expected at the sediment scale.

[23] The  $\text{CH}_4\text{-CO}_2$  exchange rate is faster than the rate of  $\text{CH}_4$  hydrate formation (data in Figures 3b and 3c), and there is additional volume expansion (compare pictures traced in Figures 4c and 4d). Both observations point toward the formation of a porous and pervious  $\text{CO}_2$  hydrate shell, probably due to the liberation and expansion of  $\text{CH}_4$  gas.

## 5. Conclusions

[24] Pore-scale electrical resistance and relative stiffness measurements provide unique insight into hydrate formation,  $\text{CH}_4\text{-CO}_2$  replacement, and hydrate dissociation.

[25] In the absence of fluid flow, CH<sub>4</sub> hydrate formation is diffusion-controlled initially through the water phase until hydrate forms. Thereafter, CH<sub>4</sub> must diffuse through the hydrate mass to reach any isolated free water that is surrounded by hydrate. Consequently, free water can remain in an excess CH<sub>4</sub> gas system for a relatively long time.

[26] Hydrate formation is much slower than thermal diffusion limited ice melting (at mm scale). Therefore, hydrate formation is not concurrent with ice melting within hydrate stability field conditions in most laboratory situations.

[27] Both CH<sub>4</sub> hydrate formation and CH<sub>4</sub>-CO<sub>2</sub> replacement cause pronounced volume expansion. During replacement, the newly formed CO<sub>2</sub> hydrate shell must be fractured or porous in order to allow for the high exchange rates observed in this study.

[28] While CH<sub>4</sub>-CO<sub>2</sub> replacement requires the opening of the hydrate cage (i.e., a solid-liquid-solid transformation), both electrical resistance and relative stiffness measurement suggest that CH<sub>4</sub>-CO<sub>2</sub> replacement occurs locally and gradually so that the overall hydrate mass remains solid and no stiffness loss should be expected at the sediment scale.

## Notation

- $\alpha$  Ratio between the mechanoelectric and electro-mechanical piezocrystal effects.
- $\rho$  Electrical resistivity ( $\Omega\text{m}$ ).
- $B$  Bulk modulus (Pa).
- $V$  Voltage (V).
- $P$  Pressure (Pa).
- $T$  Temperature (K).
- $n$  Stoichiometric ratio.
- $\delta$  Displacement (m).
- $k$  Stiffness (N/m).
- $L$  Height (m).
- $A$  Area (m<sup>2</sup>).
- $E$  Young's modulus (Pa).
- $\beta$  Shape factor.

## Acknowledgments

[29] Support for this research was provided by U.S. Department of Energy. Additional funding was provided by the

Goizueta Foundation. We are grateful to Connor Barrett for proofreading the manuscript.

## References

- Collett, T. S. (2002), Energy resource potential of natural gas hydrates, *AAPG Bull.*, *86*, 1971–1992.
- Davies, S. R., et al. (2008), A novel approach to measuring methane diffusivity through a hydrate film using differential scanning calorimetry, paper presented at the 6th International Conference on Gas Hydrates, U.S. Dep. of Energy, Vancouver, B. C., Canada.
- Donnelly, H. G., and D. L. Katz (1954), Phase equilibria in the carbon dioxide-methane system, *Ind. Eng. Chem.*, *46*, 511–517, doi:10.1021/ie50531a036.
- Jung, J. W., D. N. Espinoza, and J. C. Santamarina (2010), Properties and phenomena relevant to CH<sub>4</sub>-CO<sub>2</sub> replacement in hydrate bearing sediments, *J. Geophys. Res.*, *115*, B10102, doi:10.1029/2009JB000812.
- Kvenvolden, K. A. (1988), Methane hydrate—A major reservoir of carbon in the shallow geosphere?, *Chem. Geol.*, *71*, 41–51, doi:10.1016/0009-2541(88)90104-0.
- McGrail, B. P., et al. (2007), Using Carbon Dioxide to Enhance Recovery of Methane from Gas Hydrate Reservoirs, *Final Summary Rep.*, PNNL-17035, Pac. Northwest Natl. Lab., U.S. Dep. of Energy, Richland, Wash.
- Milkov, A. V. (2004), Global estimates of hydrate-bound gas in marine sediments: How much is really out there?, *Earth Sci. Rev.*, *66*, 183–197, doi:10.1016/j.earscirev.2003.11.002.
- Ota, M., et al. (2005), Replacement of CH<sub>4</sub> in the hydrate by use of liquid CO<sub>2</sub>, *Energy Convers. Manage.*, *46*, 1680–1691, doi:10.1016/j.enconman.2004.10.002.
- Ota, M., et al. (2007), Macro and microscopic CH<sub>4</sub>-CO<sub>2</sub> replacement in CH<sub>4</sub> hydrate under pressurized CO<sub>2</sub>, *AIChE J.*, *53*, 2715–2721, doi:10.1002/aic.11294.
- Park, Y., et al. (2006), Sequestering carbon dioxide into complex structures of naturally occurring gas hydrates, *Proc. Natl. Acad. Sci. U. S. A.*, *103*, 12,690–12,694, doi:10.1073/pnas.0602251103.
- Ruppel, C., and J. W. Pohlman (2008), Climate change and the global carbon cycle: Perspectives and opportunities, in *Fire in the Ice: Winter 2008 Methane Hydrate Newsletter*, pp. 5–8, Natl. Energy Technol. Lab., Off. of Fossil Energy, U.S. Dep. of Energy, Albany, Ore. (Available at <http://www.netl.doe.gov/technologies/oil-gas/publications/Hydrates/Newsletter/HMNewsWinter08.pdf#page=5>)
- Stevens, C. J., et al. (2008), Experimental hydrate formation and gas production scenarios based on CO<sub>2</sub> sequestration, paper presented at the 6th International Conference on Gas Hydrates, U.S. Dep. of Energy, Vancouver, B. C., Canada.
- Svandal, A., et al. (2006), The phase-field theory applied to CO<sub>2</sub> and CH<sub>4</sub> hydrate, *J. Cryst. Growth*, *287*, 486–490, doi:10.1016/j.jcrysgro.2005.11.071.
- Zhou, X. T., et al. (2008), Determination of appropriate condition on replacing methane from hydrate with carbon dioxide, *Energy Convers. Manage.*, *49*, 2124–2129, doi:10.1016/j.enconman.2008.02.006.